JOURNAL OF SPACECRAFT AND ROCKETS
Vol. 43, No. 6, November–December 2006

Web-Based Computational Investigation of Aerothermodynamics of Atmospheric Entry Vehicles

Dr. Periklis Papadopoulos* and Prabhakar Subrahmanyam†
San Jose State University, San Jose, California 95192

DOI: 10.2514/1.19960

An entry vehicle design framework is presented in this publication that investigates the aerothermodynamics of atmospheric vehicles and provides a computational database framework for planetary probes. A platform-independent graphical user interface-based preliminary design tool, HyperProbe, has been developed and integrated to a planetary probe database to do trajectory analysis, study aerodynamic heating, and dynamic thermal protection system sizing. A comprehensive relational database management system for several atmospheric entry vehicles has been developed for comparative data analysis capability. The database comprises vehicle dimensions, trajectory data, aerothermal data, and material properties like carbon, silicon, and carbon-phenolic based ablators for several ballistic entry vehicles. HyperProbe graphical user interface provides capabilities to choose from a list of flight vehicles or enter trajectory and geometry information of a vehicle in design. An empirical model of the general atmospheric model for Earth is developed to calculate pressure, density, temperature, Reynolds number, and speed of sound as a function of altitude. Global reference atmospheric models have been used for other planetary atmospheres. A fourth-order Runge–Kutta integration is employed for trajectory calculations. Fay–Riddell, Sutton–Graves, and Tauber–Sutton empirical correlations have been modeled for the stagnation-point convective and radiative heat transfer computations.

Nomenclature

C_p	=	specific heat at constant pressure, kJ/(kg · K)
C_v	=	specific heat at constant volume
d	=	differential in Eqs. (1a–1d)
g	=	acceleration due to gravity
h	=	altitude
Kn	=	Knudsen number
Le	=	Lewis number
m	=	entry mass, Kg
M	=	Mach number
p	=	pressure, N/m^2
Pr	=	Prandtl number
$\dot{q}_{\text{conv}}$	=	convective heat transfer rate, W/cm^2
$\dot{q}_{\text{rad}}$	=	radiative heat transfer rate, W/cm^2
$\dot{q}_{\text{tot}}$	=	total heat transfer rate, W/cm^2
Q^*	=	heat of ablation
R_b	=	forebody radius, m
R_c	=	corner radius
Re	=	Reynolds number
R_{eff}	=	effective radius
R_n	=	nose radius, m
r	=	range
S	=	base area of the capsule, m^2
$\dot{S}$	=	recession rate
t	=	time, s
T	=	temperature, K
V_∞	=	freestream flight velocity, m/s
α	=	angle of attack
β	=	ballistic coefficient, kg/m^2
γ	=	flight path angle, deg
ε	=	surface emissivity of the material
θ	=	surface area inclination angle
ρ	=	freestream density, kg/m^3
σ	=	Stefan-Boltzmann's constant
Υ	=	ratio of specific heats

Subscripts

b	=	forebody
c	=	corner
conv	=	convective
e	=	entry
n	=	nose
rad	=	radiative
tot	=	total
w	=	wall
∞	=	freestream

Received 8 September 2005; revision received 9 January 2006; accepted for publication 25 April 2006.

*Associate Professor, Center of Excellence for Space Transportation and Exploration, Department of Mechanical and Aerospace Engineering, San Jose State University, One Washington Square; ppapado1@email.sjsu.edu. Senior Member AIAA.

†Graduate Researcher & Aerospace Engineer, Center of Excellence for Space Transportation & Exploration, Department of Mechanical and Aerospace Engineering; prasub@gmail.com. Associate Member AIAA.

I. Introduction

The United States national vision for space exploration calls for "the human and robotic exploration of the solar system and beyond." Human and robotic exploration of the solar system is to search for evidence of life, to understand the history of the solar system, and to support human exploration. But before they arrive, planetary probes will likely have preceded them to provide the understanding required to make further exploration possible. Advances in technology ranging from new instrumentation, sophisticated materials, and improvised nanotechnology make planetary probes a vital tool in pursuit of scientific truth and the origins.

In support of this mission, a complete computational design framework is necessary that automates the calculations for stagnation-point heating, thermal protection system (TPS) sizing so that better probes can be built with this analysis. An integrated planetary probe design framework that automatically computes TPS sizing and surface heating given vehicle geometry and entry trajectory flight conditions is presented in this paper. The probe design framework includes access to existing probe designs and provides a mini-CAD like design environment for construction of new configurations based on classes consistent with existing designs.

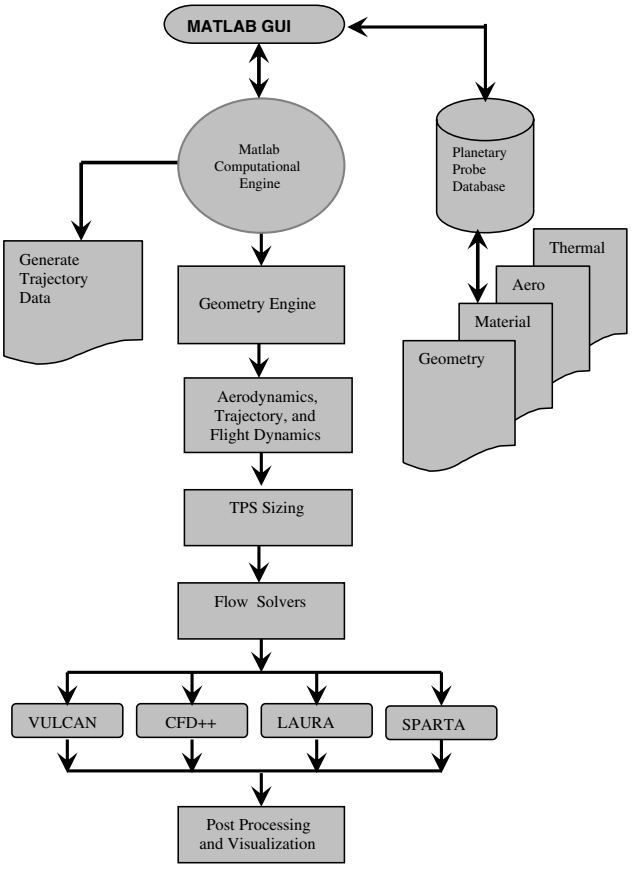

Fig. 1 HyperProbe software architecture.

A platform-independent graphical user interface (GUI) based, relational database-driven tool called HyperProbe has been developed to accurately predict aerodynamic and heating entry environments. The aeroheating environment depends on the trajectory flown, size and shape of the vehicle.

II. Software Architecture

Figure 1 shows the software architecture of HyperProbe. Once the TPS sizing is done, it can be automatically linked to CFD tools for grid generation and analysis. A comprehensive database of ballistic reentry vehicles has been developed using the "Planetary Mission Entry Vehicles" manual [1]. This includes vehicle dimensions and trajectory data for all the capsules that have been flown in the past. The HyperProbe GUI provides the capability to choose from a list of flight vehicle geometric information and entry trajectories. This tool is intended as a preliminary design framework for planetary entry vehicle design.

The overall software architecture is shown in Fig. 1. The front GUI allows the user to provide inputs for trajectory and geometry. It is connected to an extensive planetary probe database and a MATLAB computational engine, which is used to generate flight trajectory data. From the trajectory data, stagnation-point aerodynamic heating and TPS size requirements are computed. TPS sizing requires the selection of materials that effectively protect the vehicle during reentry. The database has several different categories of Ablators to choose from including carbon, reusable composites, carbon-phenolic, and silicon-based ablators.

With the emerging information technology growth, heterogeneous systems are rapidly developing and this presents a need for distributed analysis systems. With this in mind, a platform-independent tool has been developed. This architecture-neutral code has the capability to execute in any platform for analysis without having to recompile.

The GUI based analysis tool was developed in the MATLAB platform-independent environment. Figure 2 shows the probe design

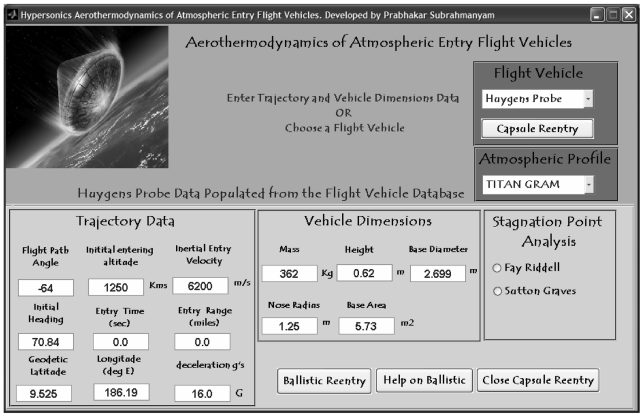

Fig. 2 HyperProbe graphical user interface.

options provided in the HyperProbe interface. A planetary probe can be chosen from the user interface (UI) flight vehicle drop-down menu. When the flight vehicle is chosen, appropriate initial trajectory, and vehicle dimensions data are populated in the input boxes from the relational database. Values in the input boxes can be changed by the user or the populated values can be used to run the trajectory simulation. The user is also able to choose a stagnation-point correlation, either Fay–Riddell [2] or Sutton–Graves [3] correlations from the interface.

The user can either choose a flight vehicle for trajectory analysis from the list of available probe designs in the planetary probe database as explained in the preceding paragraph or construct a new configuration. This is achieved by calling the geometry engine from within the GUI. After the vehicle is constructed, the trajectory is computed by calling the computational engine from within the GUI.

III. Trajectory Analysis

A. Atmospheric Model

The HyperProbe design environment also links the trajectory code to appropriate planetary empirical atmospheric models depending on the planetary probe that is chosen. The 1976 U.S. Standard Atmosphere for Earth, General Atmospheric Model for Earth (GAME), is modeled as a subroutine that calculates pressure, density, temperature, Reynolds number, and speed of sound as a function of altitude. Global reference atmospheric models (GRAM) [4] of Mars, Venus, Titan, and Neptune have been used to compute the atmospheric pressure, density, and temperature profiles.

B. Trajectory Computations

The probe model developed for this trajectory is a point-mass model with two translations and one rotation (3-DOF) around a spherical planet. It integrates the equations of motions of a vehicle on a ballistic entry trajectory so that no lift is generated and the body acts only on gravity. Figure 3 shows the various aerodynamic forces

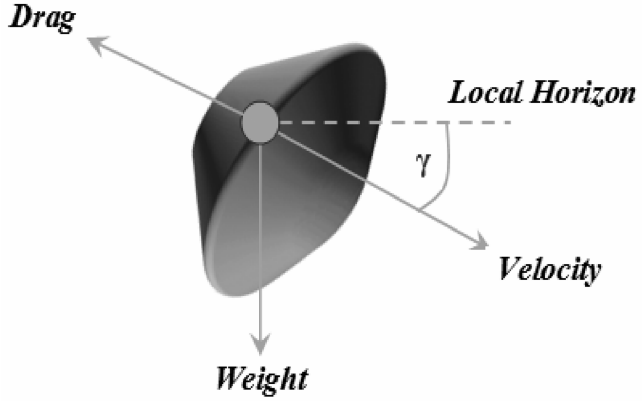

Fig. 3 Aerodynamic forces acting on the atmospheric vehicle.

Table 1 Sample output of trajectory calculated by HyperProbe

Trajectory analysis for flight vehicle: Apollo 4						
Altitude, ft	Velocity, ft/s	Flight path angle γ, deg	Mach number	Reynolds number	Stag point pressure, lbf/ft^2	Stag point heat-transfer rate $\dot{q}_{\text{conv}}$, W/cm^2
250,000.00	22,500.00	12.00	23.83	25,524.59	30.70	191.30
249,000.00	22,501.37	12.00	23.80	26,672.87	32.16	195.82
248,000.00	22,502.75	12.01	23.77	27,869.44	33.69	200.44
247,000.00	22,504.12	12.01	23.73	29,116.20	35.28	205.17
246,000.00	22,505.49	12.02	23.70	30,415.12	36.95	209.99
245,000.00	22,506.86	12.02	23.67	31,768.23	38.69	214.90
244,000.00	22,508.23	12.02	23.64	33,177.62	40.51	219.91
243,000.00	22,509.59	12.03	23.60	34,645.48	42.40	225.04
242,000.00	22,510.96	12.03	23.57	36,174.07	44.38	230.27
241,000.00	22,512.32	12.04	23.54	37,765.73	46.45	235.60
240,000.00	22,513.69	12.04	23.51	39,422.87	48.60	241.04

acting on the body. The vehicle model is built from a number of parameters defining the geometry of the probe, including body diameter, cone half-angle, nose and shoulder radius. The aerodynamic properties of the probe are subsequently derived from the geometry of the vehicle.

The Apollo capsules were chosen for demonstration of the trajectory analysis capability. Sample trajectory data is shown in Table 1 and in Fig. 4. Tables 2 and 3 show the information available in the planetary probe database.

In the example presented, the GUI is first populated with Apollo specific mission and design information retrieved from the planetary probes database. The atmospheric entry conditions and vehicle dimensions are used in the HyperProbe environment to perform the trajectory calculations. A fourth-order Runge–Kutta integration is employed for trajectory calculations to advance the solutions of differential equations to solve the following set of Eqs. (1a–1d):

$$\frac{dV}{dh} = \frac{g[(Q/\beta) - \sin(\gamma)]}{V\sin(\gamma)} \tag{1a}$$

$$\frac{d\gamma}{dh} = \frac{\cos(\gamma)[-g + (V^2/Re + h)]}{V^2\sin(\gamma)} \tag{1b}$$

$$\frac{dt}{dh} = \frac{-1}{V\sin(\gamma)} \tag{1c}$$

$$\frac{dr}{dh} = Re\frac{\mathrm{d}\theta/dt}{dh/dt} = \frac{-Re\cos(\gamma)}{(Re + h)\sin(\gamma)} \tag{1d}$$

User inputs include initial latitude, longitude, inertial velocity, reentering altitude, and initial flight path angle, and these values can be changed in the GUI if desired. The trajectory code generates the vehicle's freestream velocity, flight path angle, range, deceleration, stagnation-point heating, Reynolds number, and Mach number along the trajectory as a function of altitude. Reentry time and range are calculated as well. The trajectories computed are shown in Fig. 4 for the selected atmospheric entry conditions and the figures show the variation of flight velocity, Reynolds number, stagnation-point pressure, and deceleration against atmospheric altitude during hypersonic ballistic reentry. Tables 2 and 3, respectively, show the flight vehicle database's initial trajectory data and vehicle dimensions data that are used in the GUI and the program HyperProbe to make the trajectory calculations.

The HyperProbe design environment automatically links the 3-DOF trajectory code to appropriate empirical models of atmospheres

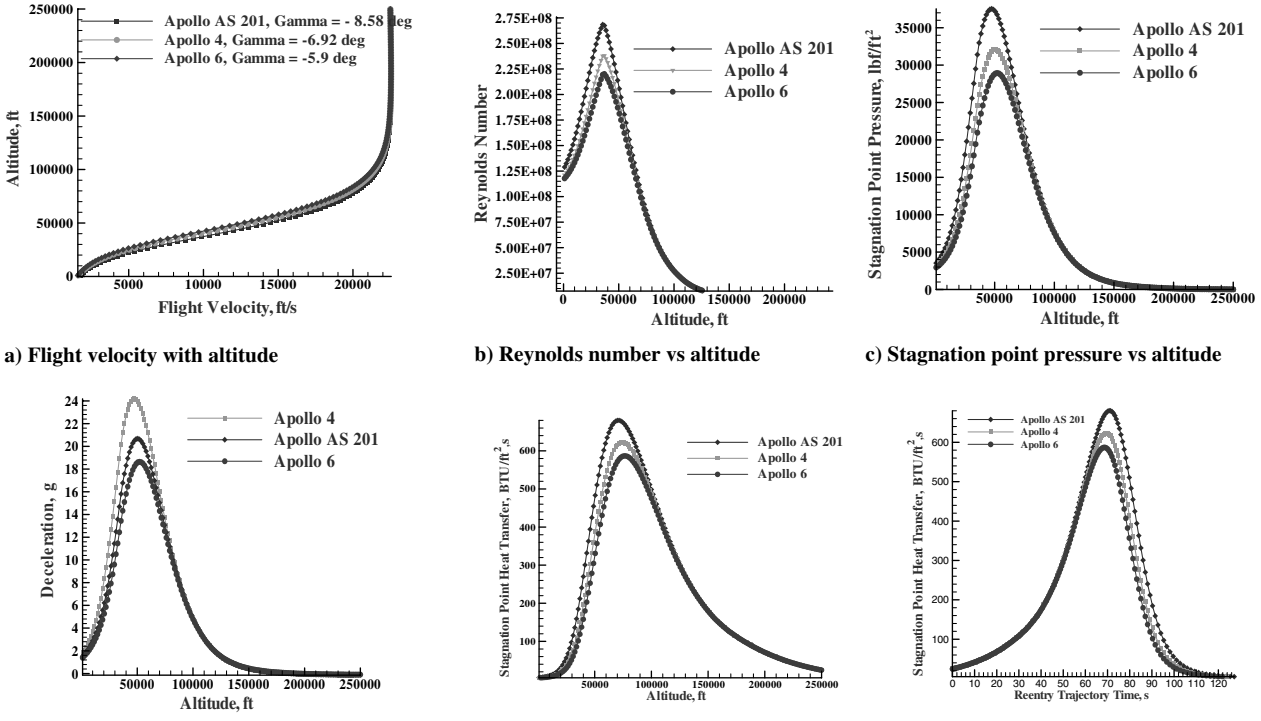

a) Flight velocity with altitude **b) Reynolds number vs altitude** **c) Stagnation point pressure vs altitude**

d) Deceleration vs altitude **e) Stagnation point heat vs altitude** **f) Stagnation point heat vs time**

Fig. 4 Trajectory data: flight velocity, stagnation-point heating, deceleration vs altitude.

Table 2 Benchmarking analysis for Apollo 6 at an entry angle of −5.9 deg

Codes	Velocity at peak heating, km/s	Altitude at peak heating, km	Maximum deceleration, g	Mach number
POST	8.45	24.01	12.15	26.40
TrajOpt	7.98	23.00	11.16	24.93
HyperProbe	8.32	23.16	11.96	26.00

Table 3 Database of entry vehicles and flight vehicle geometric dimensions

Flight vehicles	Configuration (shape)	Nose radius, m	Base area, m^2	Length, m	Diameter, m	Mass, kg
Apollo AS-202	capsule 33 deg cone	4.69	12.02	3.62	3.91	
Apollo 4	capsule 33 deg cone	4.69	12.02	3.62	3.91	5424.9
Viking I	70 deg sphere cone	0.88	9.65	1.66	3.54	980.0
Pathfinder	70 deg cone	0.66	5.52	1.508	2.65	585.3
Genesis	59.81 deg blunt cone	0.43	12.02	0.93	1.51	201.0

depending on the planet that is selected to calculate pressure, density, temperature, Reynolds number, and speed of sound as a function of altitude. The computed trajectory data can be imported for plotting and further analysis. Apollo capsules were chosen for trajectory analysis because they have identical vehicle dimensions and the plots 4a–4f show different trajectories because their initial flight path angles and ballistic coefficients are different for these flight vehicles.

Sample trajectory data are shown in Table 1. Figure 4 shows the variation of flight velocity, Reynolds number, stagnation-point pressure, and deceleration against atmospheric altitude during reentry. Three different flight vehicle trajectories have been analyzed for different values of flight path angle γ and ballistic coefficient β. Figure 4 shows Apollo AS 201 with an initial flight path angle of −8.58 deg, Apollo 4 with an initial flight path angle of −6.92 deg, and Apollo 6 with an initial flight path angle of −5.9 deg. The maximum deceleration appears at about 50,000 ft altitude close to the height of maximum stagnation-point heating load of 700 $\text{Btu} \cdot \text{ft}^2 \cdot \text{s}$ at 52,000 ft altitude.

Modified Newton flow theory (NFT) is used to evaluate the pressure coefficient C_p around the body and derive the drag coefficient C_d of the configuration. NFT follows the standard Newtonian sine-squared law, with an adjustment to give correct pressure coefficient at the stagnation-point. The modification to the Newtonian flow is represented here [Eq. (2)] in terms of the pressure coefficient

$$C_p = C_{p\,\max} \sin^2\theta \tag{2}$$

where C_p is local surface pressure coefficient

$$C_p = \frac{p - p_\infty}{(1/2)\rho_\infty V_\infty^2} \tag{3}$$

In Eq. (3), p is the local surface pressure, p_∞ is the freestream static pressure, and $q_\infty = (1/2)\rho_\infty V_\infty^2$ is the freestream dynamic pressure. The deflection angle θ is the angle between the flow and the body surface, and $C_{p\,\max}$ is evaluated as the maximum pressure coefficient found behind a normal shock wave at the stagnation point. The ballistic coefficient of the probe is derived from the aerodynamic model as per Eq. (4)

$$\beta = m/(C_d)(S) \tag{4}$$

where m is the mass and S is the section area of the body. The higher the ballistic coefficient, the higher the heat and deceleration loads. Once the ballistic coefficient is determined, HyperProbe provides a number of entry profiles for various velocities V_e and entry angles γ_e.

C. Convective and Radiative Stagnation-Point Heating Analysis

Introducing the average specific heat [3] constant Lewis and Prandtl-Number ($Le = 1$ and $Pr = 0.71$), Fay and Riddell [2] proposed an empirical correlation to define the stagnation-point heat flux (heating rate per unit area) towards a fully catalytic, hot wall. Stagnation-point heat transfer rate for Earth has been modeled using the Fay–-Riddell theory and the Sutton–Graves correlation [3] as described in Eq. (5), which gives the heat flux as

$$\dot{q}_{\text{conv}} = k\sqrt{\frac{\rho}{R_n}}\left(\frac{V_\infty}{1000}\right)^3 \tag{5}$$

where $\dot{q}_{\text{conv}}$ is the convective heat transfer rate into the flight body, per unit area, k is a constant based on the planetary atmosphere, ρ is the freestream density, and V_∞ is the flight velocity. The heating rate for $\dot{q}_{\text{conv}}$ is in W/cm^2 if the velocity is given in m/s and the density in kg/m^3. Radiative heat transfer is computed using the Tauber–Sutton radiative heating correlation for Earth and Mars [5] as given in Eq. (6):

$$\dot{q}_{\text{rad}} = C r_n^a \rho^b f(V) \tag{6}$$

where C is a constant based on the planetary atmosphere, and $f(V)$ is a tabulated function of velocity given in [5]. The total stagnation-point heat load is computed by adding the stagnation-point convective and radiative components as shown in Eq. (7):

$$\dot{q}_{\text{tot}} = \dot{q}_{\text{conv}} + \dot{q}_{\text{rad}} \tag{7}$$

The plots in Fig. 5 show the comparison of calculated radiative heating with Fire II flight data and the engineering correlations described by Tauber et al. [5,6]. The vehicle configuration for FIRE II is an axisymmetric, 66 deg sphere cone and truncated spherical forebody with a small corner radius as described in [7]. This trajectory point corresponds to the first FIRE II heat shield, with a nose radius of 0.935 m. The results from the radiative engineering correlations are tabulated in Table 4.

The convective and radiative heating correlations of Fay–Riddell [2] and Sutton–Tauber [5] can be used to calculate the stagnation-point heating rates only on a hemispherical nose, when $R_n = R_b$. When this is not the case, these correlations cannot be readily applied and an effective nose radius has to be determined to calculate the stagnation-point heating rate on a blunt body. Effective radius is the equivalent hemispherical radius which will produce the same velocity gradient as that computed for the blunt body [8]. An effective nose radius has been determined for every probe at 0 AOA. For nonspherical configurations, an equivalent hemispherical nose radius is employed to calculate the stagnation-point values of the heat transfer coefficient as shown in [9], which gives the same shock standoff distances in an adiabatic flow. It has been observed by Ellison [10] that the effective nose radius R_{eff} decreases as the nose radius decreases and as the corner radius increases.

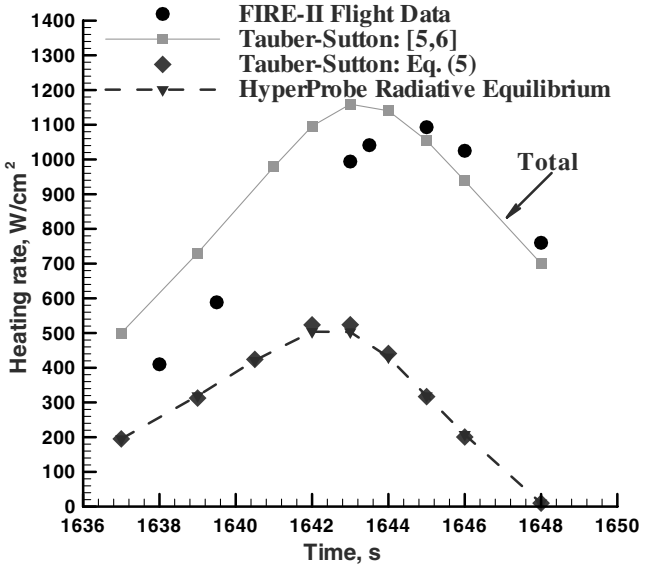

Fig. 5 Radiative stagnation-point heating of FIRE II data at a reentry velocity of 11.37 km/s.

D. Ablative Thermal Protective System Sizing and Materials Property Database

The convective and radiative heating point calculation is used to do the ablative TPS sizing. Vehicle thermal response is calculated by an approximate method that uses heat of ablation data to estimate heat shield recession during entry. This analysis is coupled to a one-dimensional finite-difference calculation that determines in-depth thermal response. The in-depth solution accounts for material decomposition, but does not account for pyrolysis gas energy absorption through the material. As inputs, the method relies on trajectory data, including relative velocity, atmospheric density, pressure, and convective heat rate as a function of time. The tool calculates radiative heating, recovery enthalpy, wall enthalpy, surface pressure, and heat transfer coefficient. Ultimately, the tool determines recession thickness, total thickness, and heat shield area mass based on thermal response at the stagnation point. A uniform thickness heat shield is modeled. In the existing atmospheric reentry relational database management system (RDBMS), a material database has been constructed and added for common ablative thermal protection and substructure materials. User-defined materials can be easily added to the database without having to modify the thermal protection systems subsection code of the reentry tool.

Stored constants for ablative materials include the decomposition kinetic constants used in the Arrhenius formulation for density decomposition, the resin volume fraction, the heats of formation, thermal conductivity, specific heat, emissivity, and heat of ablation curve fit constants. There are two components to the approximate technique presented here. The first component makes use of a steady-state ablation assumption and employs the heat of ablation Q^* to estimate recession during entry. The second component involves calculating the in-depth temperature response to predict the amount of material required as insulation to keep the bondline temperature below a specified limit. Calculating the in-depth temperature response is accomplished using a finite-difference formulation for the in-depth conduction through the material. Using the heat of ablation, the recession rate at any instant in time can be calculated by Eq. (8). The total recession is then found by integrating the recession rate over the entire trajectory. This formulation is conservative and will generally overpredict recession rate.

$$\dot{S} = \frac{\dot{Q}_{hw}}{\rho Q^*} \tag{8}$$

where $\dot{Q}_{hw}$ is the hot wall heat flux.

The one-dimensional heat conduction equation can be written, along with the surface energy balance, as shown in the following Eqs. (9) and (10):

$$\rho C_p \frac{\partial T}{\partial t} = \frac{1}{A}\frac{\partial}{\partial x}\left(\kappa A \frac{\partial T}{\partial x}\right) \tag{9}$$

$$\dot{q}_{\text{conv}} + \alpha \dot{q}_{\text{rad}} - \dot{q}_{\text{cond}} - \varepsilon \sigma T_w^4 = 0 \tag{10}$$

where T_w is the surface temperature, κ is the thermal conductivity, x is measured from TPS surface, ρ is the instantaneous material density, C_p is the material specific heat, and α is the material absorptivity.

Table 5 shows the thermal and material properties for Avcoat-5026-39 as described in [9] and reinforced carbon–carbon (RCC). Because of the high thermal conductivity of the nose cap wall and the thinness of the wall when compared with the radius of the nose cap, the Biot number is small and the nose cap wall is effectively modeled as a "lumped-mass" structure with constant temperature throughout. The material database contains carbon, silicon, and carbon-phenolic based ablators which are populated in the graphical user interface. During the probe design phase, the user can select from the list of ablators as the heat shield.

The wall thickness is defined as the depth of the ablative layer and the RCC thickness, and the average head capacity of the wall is the thickness weighted heat capacity of the ablative and RCC wall layers. The lumped-mass temperature approximation for this wall segment can be written as

$$\dot{q}_{\text{in}} - \dot{q}_{\text{out}} = [\rho_{\text{Avcoat}} C_{p\text{Avcoat}} t_{\text{Avcoat}} + \rho_{\text{RCC}} C_{p\text{RCC}} t_{\text{RCC}}]\dot{T}_w \tag{11}$$

where $\dot{q}_{\text{in}}$ is the heat flux into the wall, $\dot{q}_{\text{out}}$ is the heat flux out of the wall, $\dot{T}_w$ is the time rate of change of the wall temperature, and the remaining terms in the brackets are the average heat capacity of the wall segment. Variations of heat capacity are due to changes in the

Table 4 Stagnation-point radiative heating rate comparisons for FIRE II

V_e, km/s	γ_e deg	$m/(C_d)(S)$, kg/m^2	V_∞, km/s	$\dot{q}_{\text{conv}}$, W/cm^2	$\dot{q}_{\text{rad}}$, W/cm^2	$\dot{q}_{\text{tot}}$, W/cm^2
11.37	−8.5	40	9.25	325	10	335
12.50	−10.0	40	10.47	510	108	618
14.26	−10.0	40	11.86	730	360	1090

Table 5 Material and thermal properties of carbon and silicon-based ablators

Material	Material type	Density ρ, kg/m^3	Thermal conductivity κ, watt/m · K	Specific heat C_p, J/kg · K
ATJ	carbon-based	1729.2	117.69	711.76
Avcoat 5026-39	silicon-based	512.6	25.0	1110.0
RCC	reusable CC	1650.2	120.0	1312.0

Table 6 Database of entry vehicles and flight trajectory data

Flight vehicles	Inertial entry velocity, km/s	Relative entry velocity, km/s	Peak heat velocity, km/s	Inertial entry angle, deg	Control method
Apollo AS-202		8.29	7.77		roll modulation
Apollo 4	11.14	10.73	10.25	−6.92	roll modulation
Viking Lander 1	4.61	4.42	4.02	−16.99	3-axis reaction control system
Pathfinder	7.26	7.48	6.61	−14.06	ballistic
Genesis	11.00	10.80	9.2	−8.00	ballistic

material thickness because the values of specific heat and density are thermal properties of the material.

IV. Benchmarking

HyperProbe has been compared and evaluated against industry standard tools like Program to Optimize Simulated Trajectories (POST) and Trajectory Optimization (TrajOpt). Table 6 shows the Apollo 6 benchmarking cases. The comparison is shown in Fig. 6. POST uses a more traditional direct shooting approach that calculates the state variables as a function of time throughout the entire trajectory and this guarantees that the physics of the problem are accurate at all times during the simulation. This makes POST a perfect candidate for benchmarking against HyperProbe.

The flight vehicle configuration that was evaluated in POST, TrajOpt, and HyperProbe for the benchmark analysis was Apollo 6 reentry profile. Velocity at peak heat was found to be 8.32 km/s in HyperProbe calculations and around 8 km/s in the other trajectory tools that were used for benchmarking.

V. Planetary Probe Relational Database and Flight Vehicle Architecture

The geometry of the flight vehicle is either constructed from the GUI for user specifications or generated from the HyperProbe database for existing probes. The user specified inputs include vehicle dimensions such as the planetary probe's nose radius, forebody conical angle, corner radius, afterbody frustum conical angle, and any additional base geometry specifications. Other design variables such as the probe mass, reference area, and ballistic coefficient are also required to define the vehicle architecture. The user must also indicate the vehicle's angle-of-attack and freestream flight conditions along the reentry trajectory.

A comprehensive database of existing planetary probe designs is provided in the HyperProbe framework. Trajectory and geometry data are stored for each probe in the database. In addition to the capsule shapes, base areas, nose radii, payload masses, and the ballistic coefficients of the probes are stored in the database. Figure 7 shows configurations generated from the database for the Pathfinder, Viking, and Apollo class vehicles. The user can modify the existing vehicle designs by changing geometric features available in the GUI.

A relational database management system has been developed to access the planetary probes database. The database extends across several tables. Tables 3 and 6, for instance, are linked through a common column, *Flight Vehicle*, as it is evident from the tables. Separate tables for the vehicle geometry, thermal protection system, trajectory, and aerodynamic data are included. The database manager allows selective data retrieval through user-entered queries.

VI. Planetary Vehicle .NET Web Application Architecture

A relational database management system, HyperProbe DB, has been developed and integrated with .NET framework for web accessibility as shown in Fig. 8. RDBMS allows data of existing planetary design to be spread out in different tables like aerothermal, geometry, materials, etc., to be linked via a column, e.g., flight vehicle.

The database manager allows selective data retrieval through .NET web application user interface as shown in Fig. 9. A planetary probes database is developed in Microsoft's SQL server and is populated via the .NET web application, which is organized according to the planetary body. Choosing a planetary body from the populated drop down list of the graphical user interface gives all the probes flown to the specific planetary body as illustrated in Fig. 10.

The .NET web application retrieves the data from the flight vehicle database and populates the browser with all the flight vehicles atmospheric entry specific to the planet. Each flight vehicle contains aerothermal, geometry and TPS information from the database and is

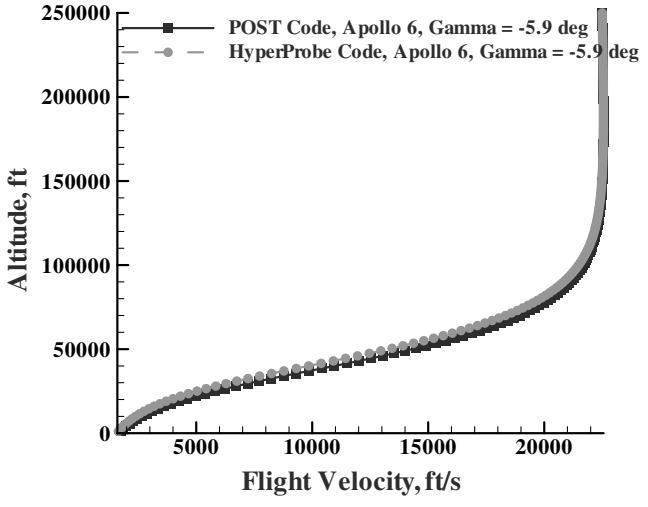

Fig. 6 HyperProbe vs POST: reentry flight velocity vs altitude.

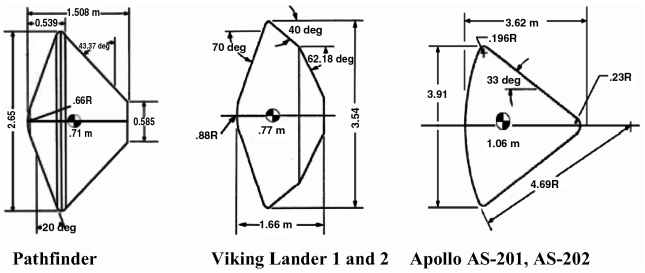

Fig. 7 Sample probe database configurations and geometry constructions as modeled in this work.

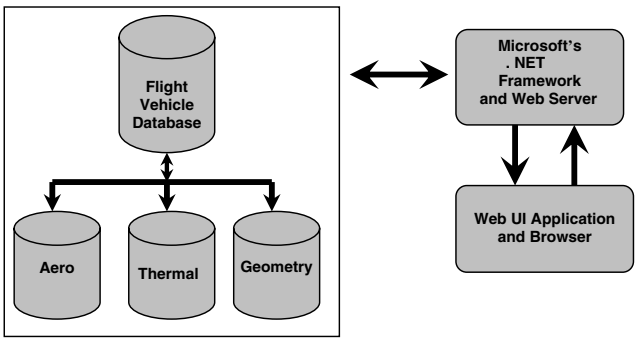

Fig. 8 Web application architecture.

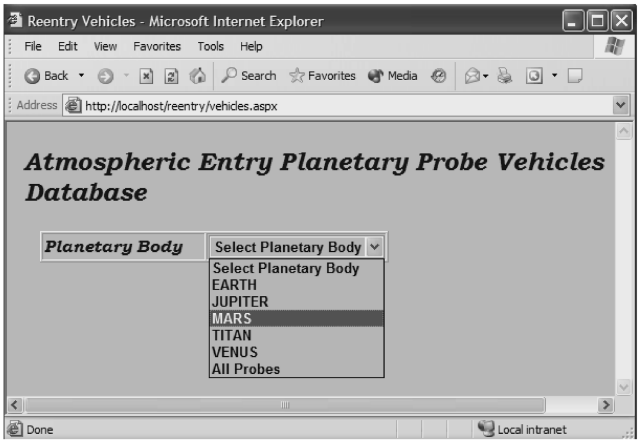

Fig. 9 Atmospheric entry .NET web user interface.

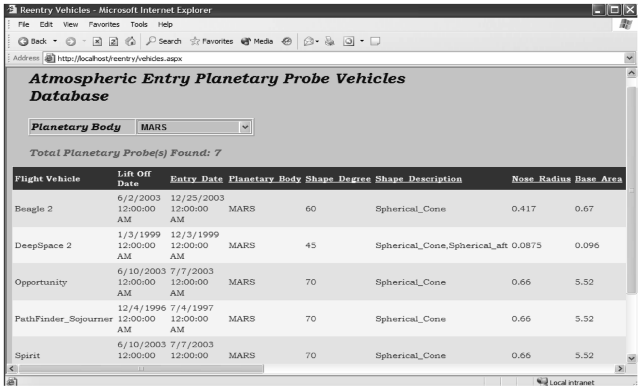

Fig. 10 Atmospheric entry planetary vehicle web application.

displayed in the web browser [11]. Clicking on the flight vehicle launches the HyperProbe GUI shown in Fig. 2. From this GUI, the 3-DOF point-mass trajectory code can be executed.

Thus, the trajectory code can be run as an independent stand-alone mode and also from the web. Trajectory code that is run from the web interfaces to the MATLAB web server as the computations are done on the server and the trajectory data are shown on the browser as a formatted HTML (hypertext markup language) output that can be saved for plotting. Stand-alone trajectory code automatically generates the trajectory data in ASCII files and also invokes the plotting utility, TecPlot [12], for plotting.

VII. Summary and Conclusions

An engineering level tool has been developed for preliminary investigation of entry vehicles. The code calculates all flight conditions along the trajectories including aerothermodynamic stagnation-point quantities and has been extensively benchmarked against industry standard trajectory codes like POST and TrajOpt. In HyperProbe, the velocity at peak heating was found to be 8.32 km/s at an altitude of 23.16 km/s for Apollo 6 type of entry vehicle at an entry flight path angle of −5.9 deg. The industry standard benchmarking tools agree with the results of HyperProbe validating the tool and works as expected for preliminary design and analysis. In addition, a comprehensive database of existing planetary probe designs is developed and integrated with the 3-DOF graphical interface tool. The flight vehicle database has been modeled and linked to the planetary probe application in .NET to be accessed from the web as well. An automated methodology of computing the stagnation-point heating and TPS sizing for the vehicle in design has been demonstrated.

Acknowledgments

The authors would like to thank Aleta Duvall of the NASA Marshall Space Flight Center for providing the Global Reference Atmospheric Models (NeptuneGRAM, VenusGRAM, MarsGRAM and TitanGRAM) for the atmospheric profiles. Thanks are also extended to Sanjeev Gupta of Intel Corporation for many helpful discussions on .NET framework for modeling the planetary probe application and extensive support in creating the SQL server database and schema for the planetary probes flight vehicles.

References

[1] Davies, C., "Planetary Mission Entry Vehicles," *Quick Reference Guide*, Ver. 2.1, NASA–Ames Research Center, 2002.

[2] Fay, J., and Riddell, F., "Theory of Stagnation Point Heat Transfer in Dissociated Air," *Journal of the Aeronautical Sciences*, Vol. 25, No. 2, Feb. 1958.

[3] Sutton, K., and Graves, R. A., "A General Stagnation Point Convective Heating Equation for Arbitrary Gas Mixture," NASA TR-376, 1971.

[4] Justus, C. G., and Johnson, D. L., "Mars Global Reference Atmospheric Model 2001 Version (MARS-GRAM 2001) User's Guide," NASA TM-2001-210961, April 2001.

[5] Tauber, M. E., and Sutton, K., "Stagnation Point Radiative Heating Relations for Earth and Mars Entries," *Journal of Spacecraft and Rockets*, Vol. 28, No. 1, 1991, pp. 40–42.

[6] Tauber, M. E., "A Review of High-Speed, Convective Heat Transfer Computation Methods," NASA TP-2914, July 1989.

[7] Cauchon, D. L., "Radiative Heating Results from the FIRE II Flight Experiment at a Reentry Velocity of 11.4 Kilometers per Second," NASA TM X-1402, July 1967.

[8] Zoby, E. V. and Sullivan, E. M., "Effects of Corner Radius on Stagnation-Point Velocity Gradients on Blunt Axisymmetric Bodies," NASA TM X-1067, 1965.

[9] NASA Ames Thermal Protective Materials and System Branch, TPS*X* Database [online database], http://asm.arc.nasa.gov [cited 14 Aug. 2005].

[10] Ellison, J. C., "Experimental Stagnation-Point Velocity Gradients and Heat-Transfer Coefficients for a Family of Blunt Bodies at Mach 8 and Angles of Attack," NASA TN D-5121, Aug. 2005.

[11] Papadopoulos, P., and Subrahmanyam, P., "Database Driven Planetary Probe Automatic Geometry and Grid Generation Tool for Atmospheric Entry Simulations," *Proceedings of the 3rd International Planetary Probe Conference*, ESA, The Netherlands; CD publication March 2006.

[12] *TecPlot® Version 9 User's Manual*, Amtec Engineering, Inc., Bellevue, WA 98009-3633, Aug. 2005.

P. Huseman
Associate Editor